Fast-ion transport in low density L-mode plasmas at TCV using FIDA spectroscopy and the TRANSP code

B. Geiger[1], A. N. Karpushov[2], B.P. Duval[2], C. Marini[2], O. Sauter[2], Y. Andrebe[2], D. Testa[2], M. Salewski[3], P.A. Schneider[1], M. Maraschek[1], the TCV Team[2] and the EUROfusion MST1 Team[4]

[1]Max-Planck-Institute for Plasma Physics, Boltzmannstr. 2, 85748 Garching, Germany
[2]Swiss Plasma Center, EPFL, Lausanne, Switzerland
[3]Technical University of Denmark, Dk-2800 Kgs. Lyngby, Denmark
[4]See appendix of H. Meyer et.al. (OV/P-12) Proc. 26th IAEA Fusion Energy Conf. 2016, Kyoto, Japan

Corresponding Author: benedikt.geiger@ipp.mpg.de

Abstract:

Experiments with 1 MW of on- and off-axis neutral beam injection (NBI) have been performed at the TCV tokamak with high electron temperatures (3-4 keV) and low electron densities (about $2\times10^{19}/\mathrm{m}^3$). Fast-Ion D-Alpha (FIDA) spectroscopy using two different optical systems observe strong signals from the fast ions that are in qualitative agreement with TRANSP/FIDASIM simulations. In addition, switching on NBI clearly reduces the loop voltage and increases the plasma pressure. However, good quantitative agreement between the experimental data and TRANSP predictions is only found when including additional fast-ion losses resulting, for instance, from anomalous fast-ion transport or charge-exchange. Strong passive FIDA radiation indicates high background neutral densities such that charge-exchange losses could be substantial. Conversely, turbulence or MHD-induced anomalous fast-ion transport could be additionally present. In particular high frequency modes are observed near the frequencies of the toroidicity induced Alfvén Eignmodes (TAEs) which might redistribute the fast particles.

1 Introduction

The behavior of fast, suprathermal particles in high temperature plasmas must be understood in view of future fusion reactors. Fast ions result from the fusion reaction and can be generated in present day devices through neutral beam injection (NBI) or ion cyclotron resonance heating (ICRH). The fast particles heat the background plasma via collisions with ions and electrons and can, in case of an anisotropic fast-ion velocity space distribution, drive non-inductive toroidal currents. In the absence of plasma instabilities

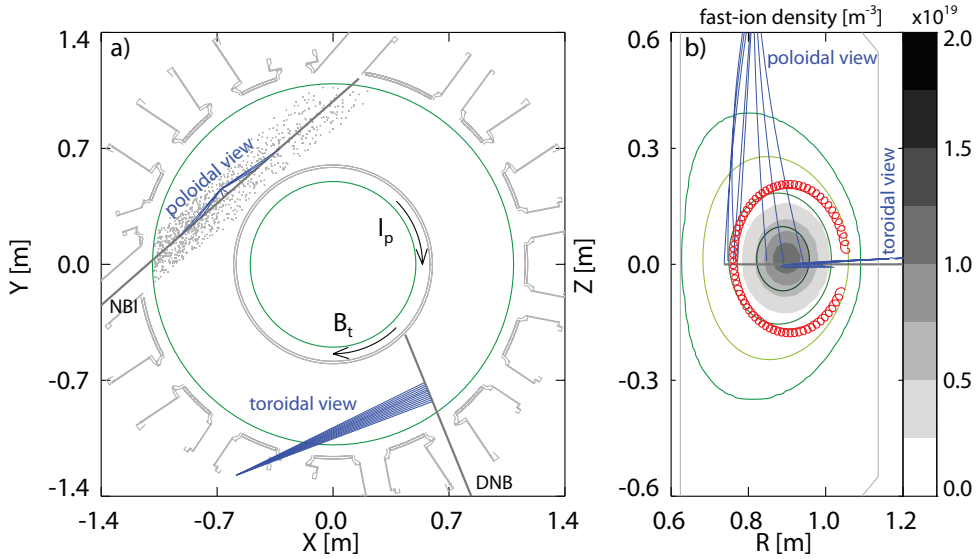

FIG. 1: Horizontal (a) and vertical (b) cuts through the TCV tokamak. The birth positions of NBI markers from a TRANSP simulation for the heating beam are illustrated in (a) by gray points. In (b), a fast-ion orbit is plotted in red that corresponds to a fast ion with 25 keV and a pitch value of 0.9 at the low field side in discharge #53783. The line of sight geometry of the FIDA diagnostic is plotted in blue in both figures.

and modes (and other anomalous transport processes), the fast-ion slowing down distribution is neoclassical and can be modeled by solving the Fokker-Planck equation, e.g. with the TRANSP code [1]. However, high temperature plasmas are not instability-free and phenomena such as Alfvén eigenmodes [2, 3, 4], sawtooth crashes [5, 6] or small-scale turbulence [7, 8] cause, so-called, anomalous transport. This affects the actual fast-ion distribution functions and must be considered when extrapolating towards future devices. The verification of theoretical models that describe the anomalous fast-ion transport is, therefore, essential and requires reliable experimental test cases. Fast-ion experiments at the TCV tokamak are particularly interesting as this device operates in a unique region of parameter space. The small size of TCV, combined with powerful ECRH and NBI heating systems, result in high fast-ion densities in presence of high electron temperatures and low plasma densities.

This paper is structured as follows. Section 2 provides details on the experimental setup at TCV, including a newly installed FIDA system. In section 3 the implementation of the TRANSP code and FIDASIM at TCV are explained. Section 4 gives the experimental results using 1 MW of on-axis and off-axis NBI. Finally, a short summary and discussion are provided in section 5.

2 Experimental Setup

The Tokamak à Configuration Variable (TCV) is a mid-size machine with major and minor radii of 0.88 m and 0.25 m, respectively. Magnetic field strengths of up to 1.5 T and currents of up to 1 MA are applied and carbon is the dominant wall material. During the experiments discussed herein, up to 1.5 MW of electron cyclotron resonance heating (ECRH) were available from three launchers, operated in second harmonic X-mode at 82.7 GHz [9]. In addition, a neutral heating beam with 1 MW of nominal power was available, injecting deuterium atoms tangentially through the plasma with a full energy of 25 keV [10]. The geometry of the NBI source and an orbit of a corresponding 25 keV ion with a pitch of $p = v_{||}/v = 0.9$ at the low field side are plotted in figure 1.

Ion temperature and rotation measurements employ charge exchange recombination spectroscopy (CXRS) on carbon ions, using a separate diagnostic neutral beam (DNB) [11]. The DNB has a power of about 60 kW and injects hydrogen neutrals at ∼49 keV. It is typically operated with 12 ms duration beam blips, separated by 24 ms to obtain accurate background subtraction for the CXRS measurement. The electron density and temperature were measured by a Thomson scattering system [12] that has 47 vertically distributed lines of sight, focused on a laser which transits from the bottom to the top of the machine. The system is typically operated with a temporal resolution of ∼17 ms and can provide full profiles for a wide range of vertical plasma displacements.

For fast particle studies, TCV is equipped with a compact neutral particle analyzer (CNPA) [13] that measures the flux of neutrals originating from charge exchange reactions between fast ions and neutrals in the plasma. In addition, a newly installed FIDA system is available, which measures Doppler shifted Balmer alpha radiation, emitted by those neutralized fast ions (based on the principle developed by [14]). For the experiments discussed here, two observation geometries are employed for FIDA spectroscopy, shown in blue in figure 1. Firstly, an array of toroidal lines of sight (toroidal view) is used that originally belonged to the CXRS system [15] and intersects the diagnostic beam (DNB). Secondly, a new system was installed that observes the heating beam from above (poloidal view). Each view is connected to a Czerny turner like spectrometer that uses two lenses with a focal length of 200 mm, a reflection grating and an EM-CCD camera, operated with a time resolution of 3 ms.

Measured spectra for one representative channel of each FIDA view are shown in figure 2. As can be seen, the toroidal system is set up to observe only up to 655 nm. This avoids the unshifted and highly intense passive D-alpha line at 656.1 nm that would cause strong detector saturation. The poloidal view, instead, observes the complete D-alpha spectrum with only modest saturation of the detector at 656.1 nm since less passive light is collected. In contrast to the toroidal view, the poloidal lines of sight feature a shorter path through the plasma (80 cm instead of 130 cm) and are less tangential to the edge region where the density of cold neutrals, emitting passive radiation, is largest.

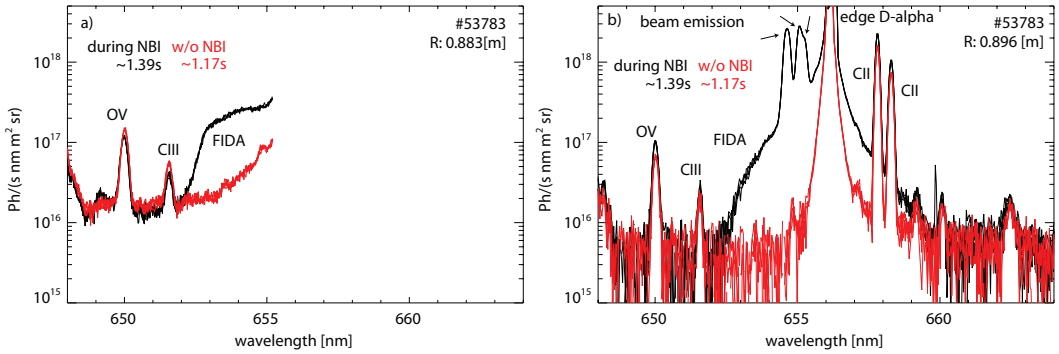

FIG. 2: Measured spectra from a central toroidal (a) and from a central poloidal (b) line of sight without (red) and with (black) the heating beam.

The spectra in red in figure 2 are without NBI while those in black are during NBI. A broad spectral component of Doppler shifted D-alpha light (FIDA) is present in both spectra with NBI. In addition, the poloidal measurement exhibits two peaks from the beam emission (full, half and one third energy component) near 655 nm. In the observed wavelength range of the toroidal system, the beam emission cannot be resolved as the Doppler shift is small (the lines of sight are almost perpendicular to the DNB). Even if the Doppler shift was larger, no beam emission and also no active FIDA radiation are expected since the presented toroidal spectrum was acquired with the DNB off. The presence of a broad spectral feature can, hence, only be explained by passive FIDA radiation, emitted by fast ions after charge exchange reactions on background neutrals. The intensity of this passive signal is stronger than the active FIDA component that originates from charge exchange reactions with neutrals present along the DNB path. To illustrate this, figure 3 shows the evolution of the integrated FIDA radiation between 653 nm and 654 nm from which an offset has been subtracted (determined at ∼651 nm). The FIDA intensity, measured by the toroidal view (figure 3b) in discharge #53694, increases when the NBI is turned on and becomes modulated slightly with the DNB power (∼5%). At about 1.63 s, the heating beam is turned off for 6 ms (see figure 3a). This causes only a modest drop in the toroidal signal, explained by its passive nature and by the relatively long slowing down time of fast ions. In contrast, the poloidal measurement (figure 3c) is strongly affected by the beam power notch because the heating beam produces much stronger active signals. The direct interpretation of the poloidal measurements is therefore simpler because the impact of passive radiation is reduced. The toroidal measurement can, in fact, be used since the modulation of the DNB permits an accurate background subtraction.

The two viewing geometries allow investigating different parts of the fast-ion velocity space as illustrated by the weighting functions [16] in figure 4 for wavelengths between 653 nm and 653.1 nm. At this blue-shifted wavelength range, the toroidal view is sensitive to co-rotating fast ions while the poloidal view is more sensitive to fast ions with small pitch values. Thus, fast-ion transport studies in different parts of the velocity space can

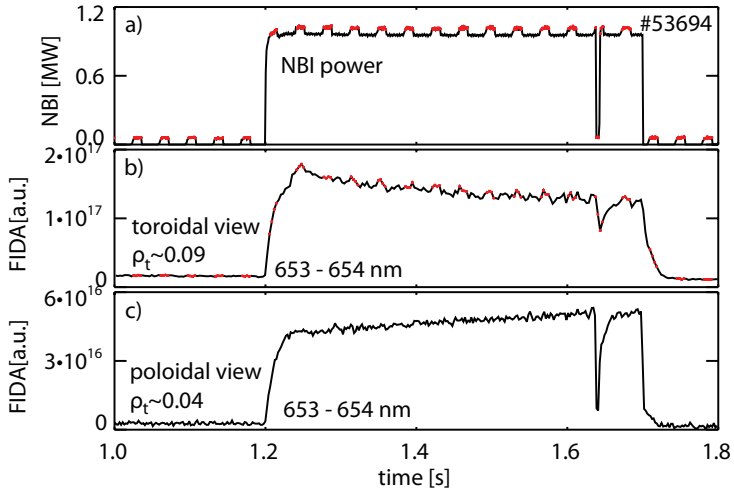

FIG. 3: Temporal evolution of the integrated FIDA signal, measured with the toroidal and poloidal systems. Phases when the diagnostic beam is on are indicated in red.

be performed.

For future experiments, it is even planned to add a toroidal view that intersects the heating beam and that will be dominated by strong active FIDA signals. Due to the better signal to noise ratio, the inference of a 2D fast-ion velocity distribution function at TCV by velocity-space tomography [17] might become possible. Figure 5 shows a comparison between the TRANSP predicted fast-ion velocity space for discharge #53783 and a tomographic inversion from synthetic FIDA spectra. 10% of Gaussian noise was added to the synthetic spectra and wavelength ranges were disgarded where the FIDA light is not observable due to the much brighter thermal charge exchange and beam emission components. For two-view FIDA systems such as the TCV one, the use of prior information is essential. We use the known position of the beam injection peaks at full-, half and one-third energy, the non-negativity of the distribution function, and the absence of FIDA light to restrict the velocity space [18]. The overall shape of the distribution function in figure 5b is well recovered from the noisy synthetic FIDA measurements in the observable wavelength regions. This indicates that a second FIDA view on the heating beam will permit to use velocity-space tomography on TCV for future studies.

3 TRANSP and FIDASIM

The TRANSP code [1] has been applied in its interpretative mode to compute neoclassical fast-ion distribution functions, as well as their impact on quantities such as the loop voltage and toroidal beta. TRANSP uses the NUBEAM [19] package to model the heating and current drive from NBI and the TORAY [20] code for ECRH and ECCD. It requires the evolution of the kinetic profiles, plasma current, toroidal magnetic field, the shape

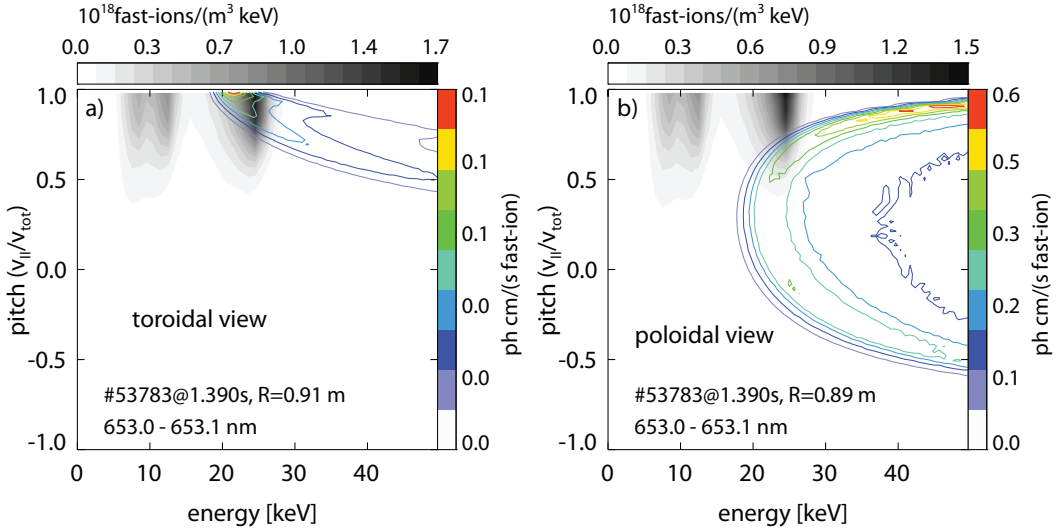

FIG. 4: Weight functions showing the observed part of the fast-ion velocity space distribution using the toroidal view (a) and the poloidal view (b). In addition, a TRANSP predicted fast-ion velocity distribution present along the line of sight is shown in gray shades.

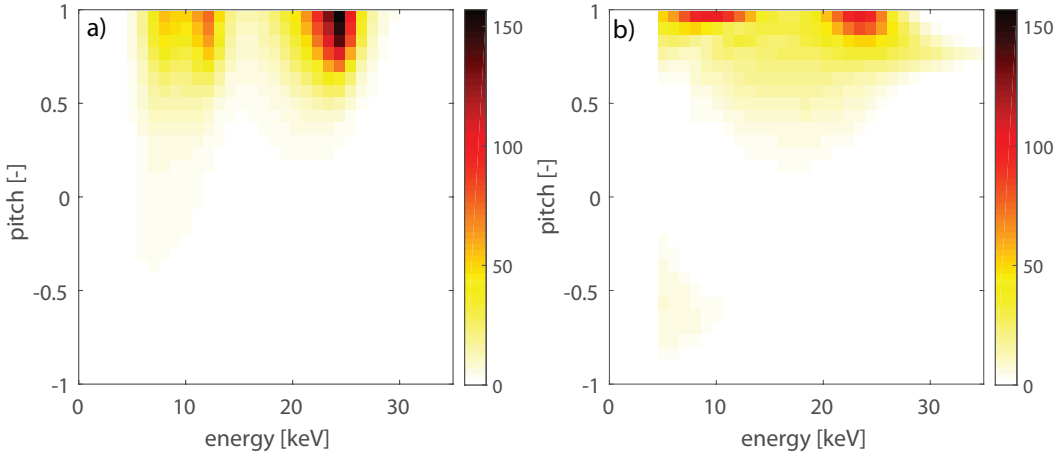

FIG. 5: (a) TRANSP simulation and (b) tomographic inversion from synthetic measurements in the experimentally accessible wavelength ranges with 10% Gaussian noise.

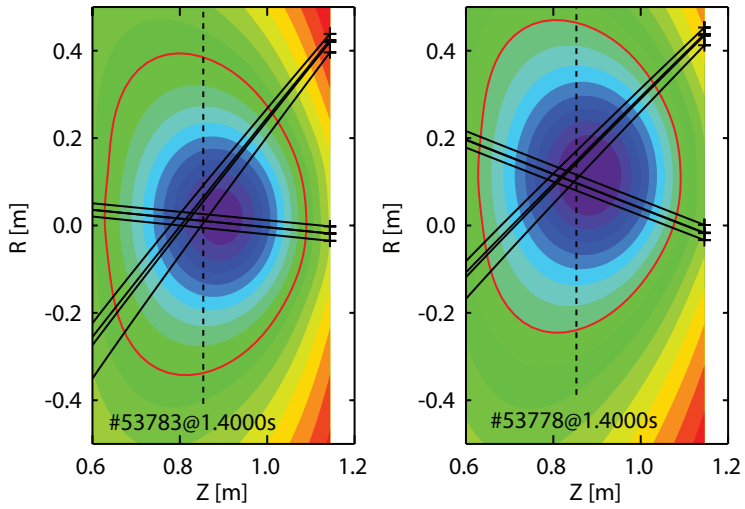

FIG. 6: Poloidal flux surfaces from TRANSP and ECRH ray geometry for discharges #53783 (on-axis) and #53778 (off-axis). The dashed vertical lines illustrate the resonance position of the ECRH radiation (82.7 GHz).

of the last closed flux surface and an initial q-profile. TRANSP then applies a time dependent equilibrium solver that considers the plasma pressure, neutral beam current drive, electron cyclotron current drive and the bootstrap current. Herein, the NBI current drive efficiency is calculated according to reference [21] with the bootstrap current and the plasma resistivity determined according to reference [22].

For TORAY, each ECRH launcher at TCV is modeled from four injection lines, each simulated by 100 rays to account for the divergence. For the experiments discussed here, a divergence of eight degrees is employed that is significantly larger than the actual divergence but is used to account for the broadening of the ECRH deposition profile by radial transport of suprathermal electrons as reported by [23]. If this effect were not considered, the equilibrium solver of TRANSP fails due to too strong and localized currents. The geometry of the injection lines of two launchers are plotted in figure 6 for two vertical plasma positions (on-axis NBI and off-axis NBI, see below).

NUBEAM calculates the NBI deposition profile, i.e. the initial location of fast ions, and subsequently solves the Fokker-Planck equation with a Monte Carlo approach in two spatial and two velocity space coordinates (R, Z, energy, pitch). It employs the NBI power, energy, species mix (68%,25%,7% for the full, half and one third energy in terms of the power) and the geometry, focus and divergence of all NBI sources. The beam species must be specified, i.e. deuterium for the heating beam and hydrogen for the diagnostic beam. We assume a rectangular shape of the heating beam even though the source is circular. This is necessary as the beam divergence is different in the horizontal and vertical planes (1.13 degree and 0.81 degree, respectively) which cannot, as yet, be simulated by NUBEAM. NUBEAM can either model a circular source with one divergence or a

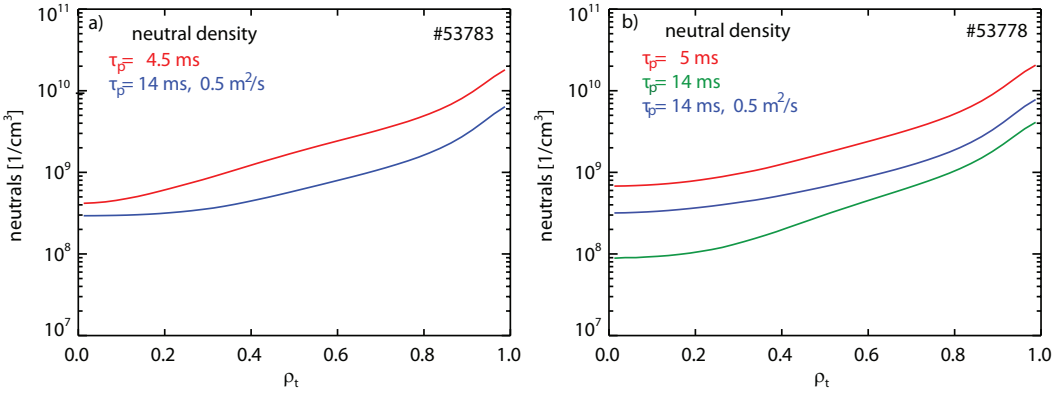

FIG. 7: Predicted radial neutral density profiles for different τ_p values during on-axis NBI (a) and off-axis (b) NBI at 1.39 s

rectangular source with separate divergences. Figure 1a illustrates resulting deposition positions of NBI markers for a simulation that is based on discharge #53783 (discussed in detail in section 4). The predicted poloidal fast-ion distribution is plotted in figure 1b in shades of gray. The fast-ion density peaks on axis when the plasma center is located around Z=0. A corresponding fast-ion velocity space distribution is shown in figure 4 that peaks at pitch values close to one. In addition, injection peaks at full, half and one third energy can be identified. To calculate fast-ion orbit losses, the first wall was approximated in the poloidal plane by 8 lines, shown in figure 1b in gray. Fast ion orbits that would intersect these lines are treated as lost.

To consider charge exchange losses with background neutrals, the background neutral density is modelled by FRANTIC [24], a 1D code that describes the penetration of neutrals sourced at the walls into the plasma. Either the recycling and gas-valve sources or the ion confinement time τ_p (used for this work) are required. τ_p allows FRANTIC to calculate the neutral density as the radial outflow of thermal ions is balanced by the ionization of neutrals (fuelling). By varying τ_p in the simulation, a range of radial neutral density profiles are obtained and shown in figure 7.

The Monte Carlo code FIDASIM [25] is now used to translate fast-ion distribution functions from NUBEAM into synthetic spectra for a given line of sight geometry. The code employs the same kinetic profiles used for TRANSP as well as the equilibrium from TRANSP. For TCV, the code was modified to be able to simulate hydrogen beams in combination with a deuterium fast-ion distribution function (the diagnostic beam injects hydrogen neutrals). Furthermore, the simulation of passive FIDA radiation was also added due to the previously discussed strong passive FIDA radiation. For the simulation of passive FIDA radiation, the code uses the background neutral density from FRANTIC and assumes that their velocity is represented by the local ion temperature. By additionally assuming that the neutrals are in the n=1 state, charge exchange rates with fast ions can be calculated. The neutralized fast ions are then followed through the 3D simulation grid

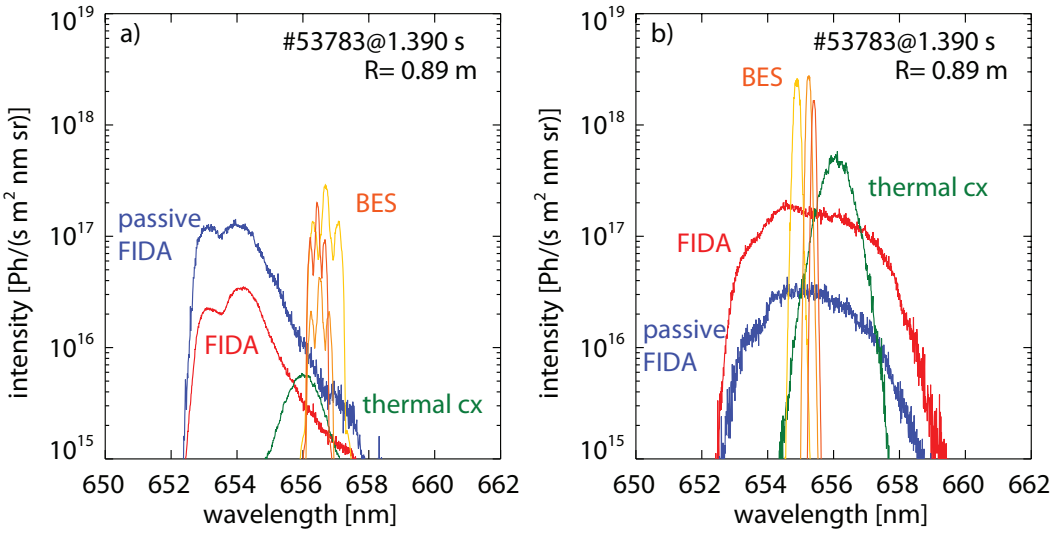

FIG. 8: Synthetic spectra of the toroidal view using the DNB (a) and of the poloidal view using the heating beam (b). The simulated spectra correspond to a TRANSP simulation for which $\tau_p = 4.5$ was assumed.

of FIDASIM and the D-alpha radiation observed along a given line of sight is determined.

Figure 8 shows simulated spectra from FIDASIM for a central toroidal line of sight and a central poloidal line of sight. The predicted beam emission, consisting of the full, half and one third energy components, exhibits stronger Doppler shifts in the poloidal measurement since the LOS geometry is more tangential to the neutral beam. The thermal charge exchange component is shown in green. Its width corresponds to the ion temperature and it is slightly blue-shifted due to the toroidal plasma rotation. The simulated active FIDA signal (red) of the poloidal view is significantly larger than that of the toroidal view since the NBI source is considerably stronger than the diagnostic beam with a corresponding increase in the neutralization rate. In contrast, a significantly stronger passive FIDA signal (blue) is expected for the toroidal view because the lines of sight are more tangential to the edge region and have a longer path within the plasma.

4 Analysis experiments with on- and off-axis NBI

Several experiments with 1 MW of NBI heating power were performed with on-axis NBI or with a vertically shifted plasma (+10 cm) to study off-axis NBI. The discharges were in limiter configuration with a clockwise directed magnetic field of 1.43 T and a clockwise directed current of 180 kA (seen from above). This corresponds to co-injected NBI with relatively small first orbit losses. Figure 9 shows time traces from two representative discharges (#53778 and #53783). The off-axis discharge #53778 ran through, while the on-axis discharge #53783 disrupted at 1.5 s due a problem with the vertical control.

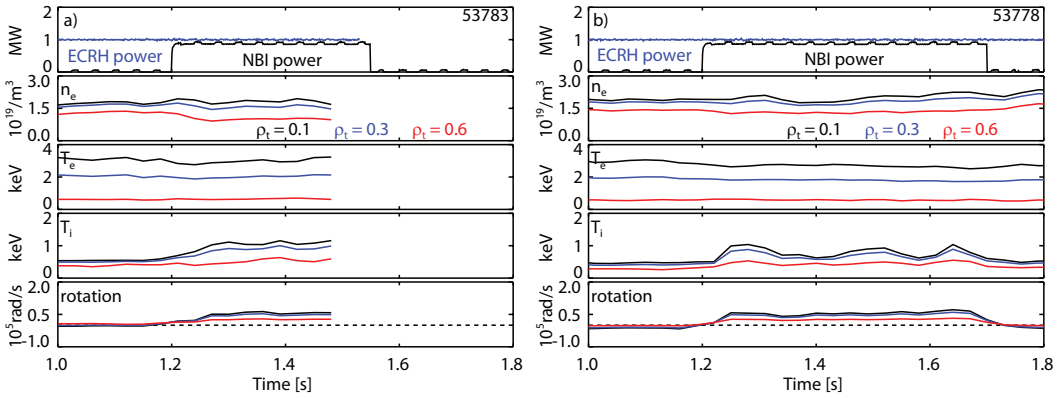

FIG. 9: Representative time traces of discharges #53783 (on-axis) and #53778 (off-axis).

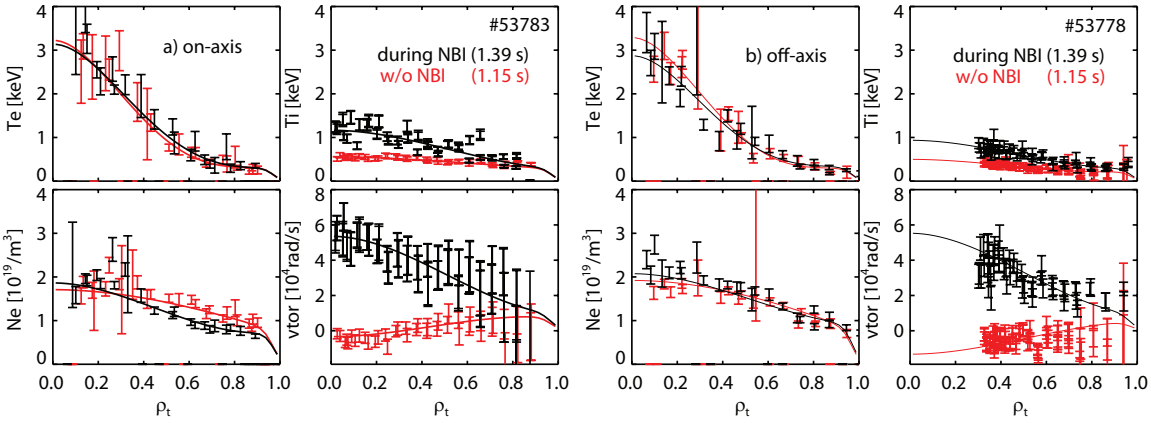

FIG. 10: Kinetic profiles measured in discharges #53783 and #53778 with (1.5 s, black) and without NBI (1.1 s, red) which have been fitted for TRANSP with a modified hyperbolic tangent function.

The discharges were heated with 1.0 MW of centrally deposited ECRH that additionally drove a counter plasma current. This procedure results in flat or reversed q-profiles and avoids sawtooth instabilities which would adversely affect the fast-ion distribution function. Between 1.2 s and 1.7 s, the heating beam was injected with 0.9 MW of power (assuming 100 kW of neutral beam losses in the beam duct) that increased the central ion temperature from ∼0.4 keV to ∼1 keV and the toroidal plasma rotation frequency from ∼-10 krad/s to ∼60 krad/s. The electron temperature almost remains unaffected during NBI as ion heating dominates at high electron temperatures [26].

For the interpretation of the discharges, several TRANSP simulations were performed for a range of background neutral densities (i.e. charge exchange losses) and anomalous fast-ion transport. The background neutral density profiles considered here are displayed in figure 7 and correspond to different τ_p values. It should be noted that the assumption of anomalous fast-ion diffusion changes the neutral density for a given τ_p. The higher

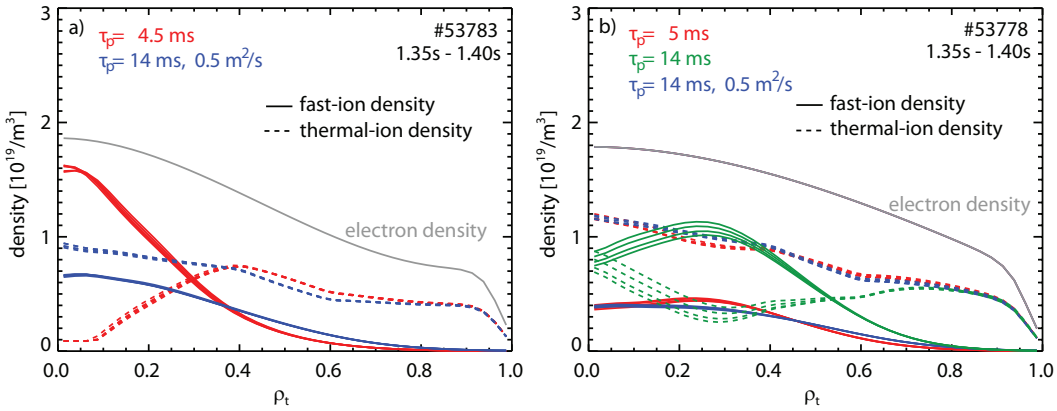

FIG. 11: Electron density profiles (gray) compared with radial fast-ion density profiles assuming 5 ms of ion-confinement time (red), 14 ms of ion confinement time (green) and 14 ms of ion confinement time plus anomalous fast-ion transport. The dashed lines correspond to the calculated thermal Deuterium ion density.

the level of anomalous fast-ion transport, the lower the fast-ion fraction in the plasma, the higher the thermal ion density, the higher the thermal ion outflow across the plasma boundary and, thus, more background neutrals are needed to obtain particle balance.

In absence of the heating neutral beam, the effective charge profile required by TRANSP was assumed constant over the radius and in time and was determined by matching predicted and measured loop voltages during ohmic plasma conditions (Z_{eff}=3). During heating beam operation, a hollow Z_{eff} profile is assumed (Z_{eff}=3 at the plasma edge and Z_{eff}=1.6 in the center) which is in qualitative agreement with CXRS measurements (carbon impurity profiles from relative intensities) and also agrees with measurements of the central Z_{eff} value based on soft X-ray data. This hollowness of Z_{eff} is expected since the heating beam fuels the plasma significantly which dilutes the impurities.

To illustrate the sensitivity of the fast-ion density prediction to τ_p and the anomalous fast-ion transport, figure 11 shows radial fast-ion densities during on-axis NBI and off-axis NBI assuming τ_p of 5 ms and 14 ms. During on-axis NBI, $\tau_p = 4.5$ ms was required as with $\tau_p = 5$ ms, TRANSP stops the simulation with a negative thermal deuterium ion density. This is given by the electron density minus the impurity density and minus the fast-ion density and is shown by dashed lines in figure 11. The thermal deuterium density profile is clearly close to zero in the center for $\tau_p = 4.5$ ms and also for $\tau_p = 14$ ms during off-axis NBI (#53778) almost no thermal deuterium ions remain. When considering $\tau_p = 14$ ms and additionally adding anomalous fast-ion diffusion of $0.5m^2/s$ (constant in real and velocity space), flattened radial fast-ion density profiles are obtained (shown in blue).

The assumption of high neutral densities at TCV reduces the fast-ion density due to charge-exchange losses. The fast NBI ions undergo a charge exchange reaction and leave the plasma as neutrals, heating the first wall instead of the plasma. This yields

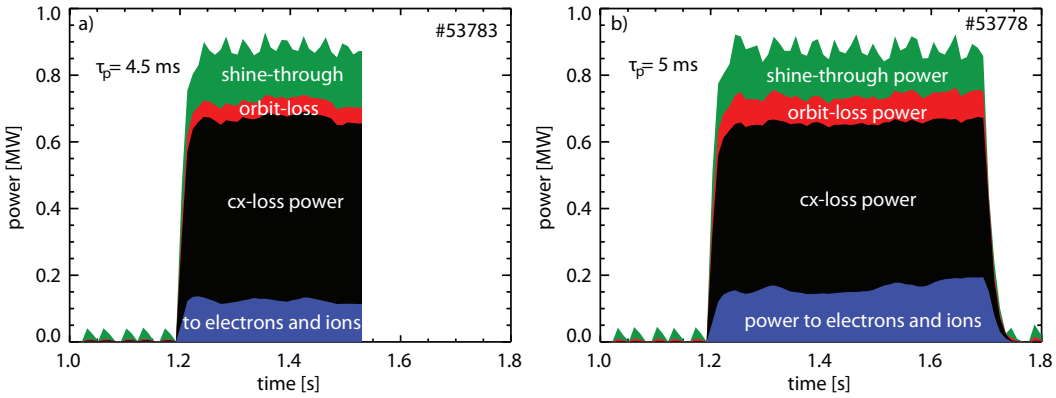

FIG. 12: TRANSP predicted power to electrons and ions, charge exchange losses, orbit losses and shine through power in discharges #53783 (on-axis) and #53778 (off-axis).

a strong reduction of the heating power of the thermal background plasma. When, e.g. considering τ_p of about 5 ms, up to 500 kW are lost by charge exchange as indicted in figure 12. In addition, orbit losses (about 50 kW) and shine-through losses (about 200 kW) are considered by TRANSP, which yields only about 150 kW of heating power applied on thermal ions and electrons.

This result can now be probed using the FIDA measurement. Figure 13 shows active FIDA spectra from four lines of sight of the poloidal view (the background radiation has been subtracted). In addition, predictions from FIDASIM, based on the TRANSP predicted fast-ion distribution functions, are shown. Unfortunately, we could not obtain an absolute intensity calibration of the FIDA system due access limitations into the TCV vessel. However, the poloidal measurement can be calibrated by matching the predicted beam emission with the data. By applying a single calibration factor to the whole system (1.05×10^{13}), good agreement is found between all channels and the simulated beam emission.

The simulation plotted in red corresponds to the neoclassical simulation assuming $\tau_p \approx$ 5 ms. Apart from the on-axis case in the very center (ρ_t=0.05), this assumption provides a good match with the data. In blue, the synthetic FIDA spectra are plotted that correspond to the TRANSP simulation with anomalous transport. Here, also, good agreement with the experimental spectra is obtained. In contrast, the neo-classical simulation for the off-axis case assuming $\tau_p = 14$ ms (green) clearly overestimates the measured signal. This corroborates the assumption of reduced fast-ion densities, either purely caused by charge exchange losses or caused by weaker change exchange losses in combination with anomalous fast-ion transport.

The presence of strong neutral densities that cause charge exchange losses is also supported by the measurement of passive FIDA radiation from the toroidal view. Figure 14 compares an active (black) and passive (blue) spectrum with the prediction from

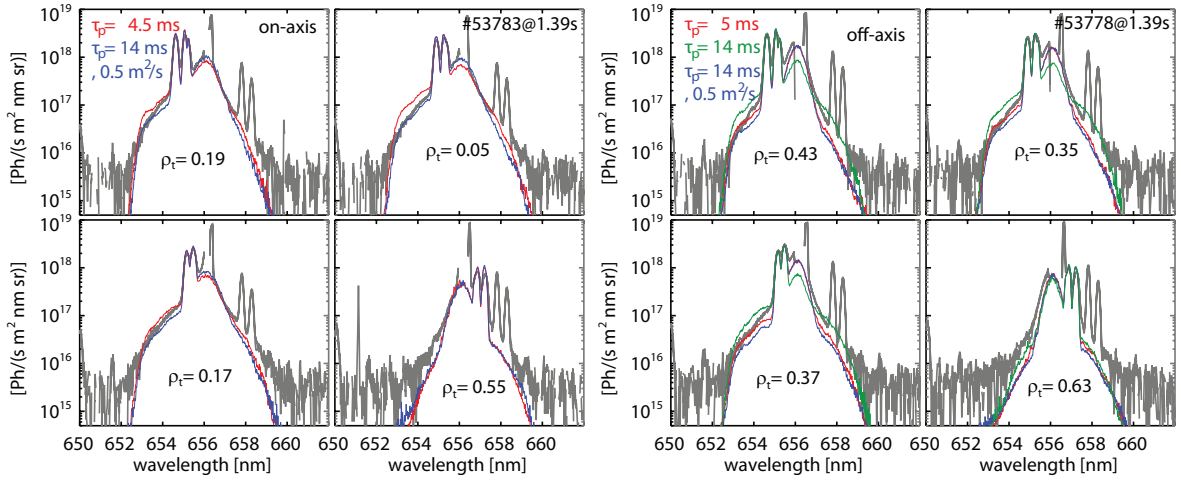

FIG. 13: a) Active FIDA spectra from four poloidal spectra during on-axis NBI (a) and during off-axis NBI (b). In addition, predictions from FIDASIM are plotted that are based on different TRANSP simulations.

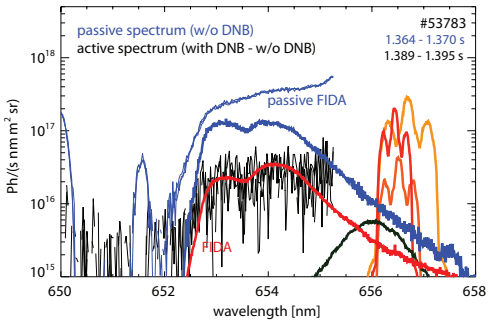

FIG. 14: Active and passive toroidal FIDA spectrum compared with predictions from FIDASIM.

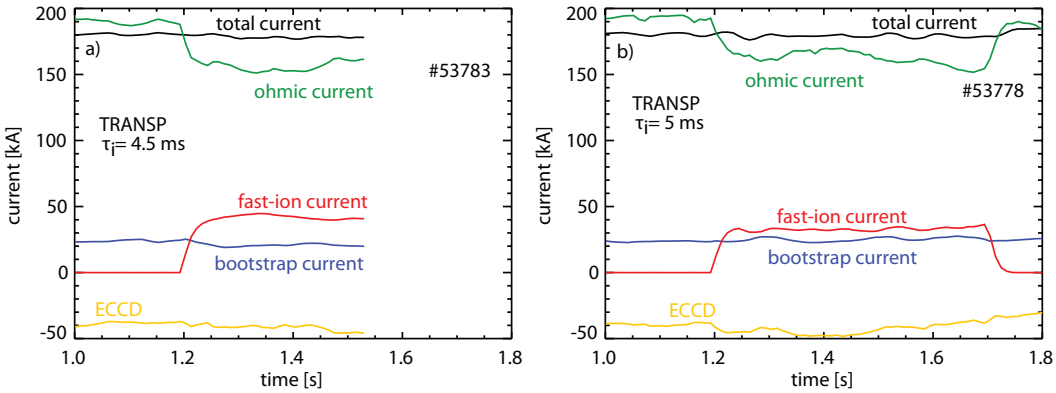

FIG. 15: TRANSP predicted temporal evolution of the different contributions to the plasma current in discharges #53783 (on-axis) and #53778 (off-axis).

FIDASIM that represents the TRANSP simulation with $\tau_p = 4.5$ ms for discharge #53783. The active emission corresponds to spectra during DNB operation after subtraction of DNB-free time frames. The toroidal measurement lacks an intensity calibration so the data is scaled (factor 1×10^{13}) to match the active FIDA prediction (red). In addition to the active component, the much stronger passive radiation is plotted in blue. This large passive signal can be reproduced well by FIDASIM using the background neutral density from FRANTIC. This demonstrates that the ratio of active to passive radiation is consistently modeled and that large neutral densities exist in these TCV experiments. A factor of two would provide a better match between the measured and synthetic passive signals but remains within the uncertainties of the model. The neutral density considered by TRANSP and FIDASIM is constant on flux surfaces which is typically not the case in tokamak plasmas. Moreover, FIDASIM does not consider fast ions outside the plasma boundary neglecting a possible contribution of passive FIDA radiation from that region.

In addition to the FIDA measurement, the TRANSP simulation validity can also be assessed by investigating the NBI current drive efficiency. In figure 15, the predicted evolution of the contributions to the plasma current are displayed for $\tau_p \approx 5$ ms with no anomalous fast-ion transport. As can be seen in figure 15, the bootstrap current and ECCD remain constant throughout the displayed time window while the fast-ion current increases to about 40 kA with NBI heating. During the NBI phase the ohmic current, necessary to maintain the regulated total plasma current, reduces accordingly.

The predicted reduction of the ohmic current is monitored experimentally by the loop voltage, plotted in figure 16. The reduction of the measured loop voltage during NBI is in good agreement with TRANSP for $\tau_p \approx 5$ ms and for the simulations that include anomalous fast-ion transport of $0.5m^2/s$ and $\tau_p \approx 14$ ms. By setting the simulated fast-ion current to zero, the predicted loop voltages (shown in yellow) do not drop as strongly during the NBI phase. This shows that the drop can not be solely ascribed to changes in kinetic profiles and, thus, supports an effective fast-ion current drive at TCV.

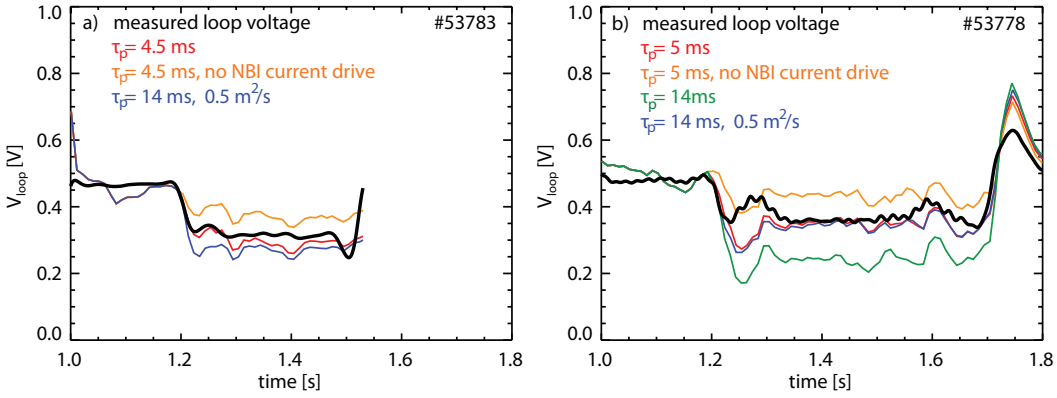

FIG. 16: Measured and predicted loop voltage in discharges #53783 (on-axis) and discharge #53778 (off-axis).

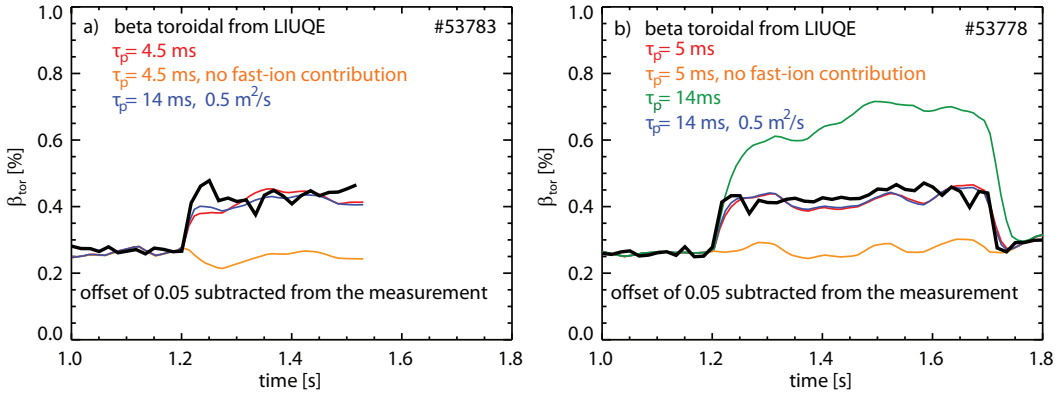

FIG. 17: Measured and predicted toroidal beta in discharges #53783 (on-axis) and #53778 (off-axis).

A similar behavior can be seen in the measured toroidal beta from the equilibrium reconstruction, i.e. the ratio of the perpendicular contribution of the plasma pressure to the toroidal magnetic field pressure. Figure 17 plots the toroidal beta when switching on NBI. The increase is caused by the fast ions and is well described by the TRANSP simulation for $\tau_p \approx 5$ ms. No increase is predicted without the fast-ion contribution (yellow simulations). This implies that the NBI-induced increase of the thermal plasma pressure is marginal. Only the presence of the fast-ions increases the toroidal beta significantly. As with the FIDA diagnostic, the simulation for $\tau_p = 14$ ms in combination with anomalous fast-ion transport can also explain the experimental data. With $\tau_p = 14$ ms and neoclassical fast-ion confinement during off-axis NBI, the loop voltage and the toroidal beta value are overpredicted.

The particle confinement time of about 5 ms, for which we obtain a good match between the measured and simulated data, is close to the global energy confinement time. This can be estimated by dividing the thermal plasma stored energy w_{th} (4.9 kJ (on-axis) and 4.7 kJ (off-axis)) by the total heating power calculated by TRANSP (for $\tau_p \approx 5$ ms) (1.1 MW (on-axis) and 1.2 MW (off-axis)). This yields an energy confinement time of 4.4 ms and 4.0 ms for on-axis and off-axis NBI, respectively. This gives the lower boundary of what one might expect for the particle confinement time since energy transport is typically higher than particle transport. The measured increase of w_{th} following NBI heating switch-on also permits an independent estimation of the NBI power coupled to the thermal plasma. By combining the low NBI heating power predicted by TRANSP (for $\tau_p \approx 5$ ms) with the Kaye L-mode scaling [27] where $w_{\mathrm{th}} \propto P^{-0.72}$ is expected, one obtains that the ion temperature during on-axis NBI should be 50% higher than measured and 25% higher during off-axis NBI. These values remain roughly within the uncertainties of the ion-temperature measurement and show that the predicted fast-ion losses by anomalous transport and/or by charge exchange losses are realistic. Even stronger losses would be required to fully match the measured ion temperature with the scaling.

Absolutely calibrated measurements from a compact neutral particle analyzer (CNPA[13]) agree with the assumption of large fast-ion densities in the plasma edge region. The CNPA yields an edge neutral density of $0.8 \times 10^{16}/m^3$ for the on-axis case and $3 \times 10^{16}/m^3$ for the off-axis case which remain in the range of neutral densities found from the TRANSP analysis. This suggests that the predicted neutral density is of the right order of magnitude and charge exchange losses clearly play an important role in fast-ion confinement for low density L-mode plasmas.

It is not possible to discriminate between only charge-exchange-induced losses and a combination of charge-exchange losses and an anomalous fast-ion transport. Possibly, high frequency modes, present in both discharges, are responsible for enhanced fast-ion transport. Figure 18 shows magnetic fluctuation spectrograms that feature weak magnetohydrodynamic (MHD) activity with a toroidal mode number of $n = 1$ at 10 kHz that disappears with NBI. In the frequency band between 50 kHz and 100 kHz modes

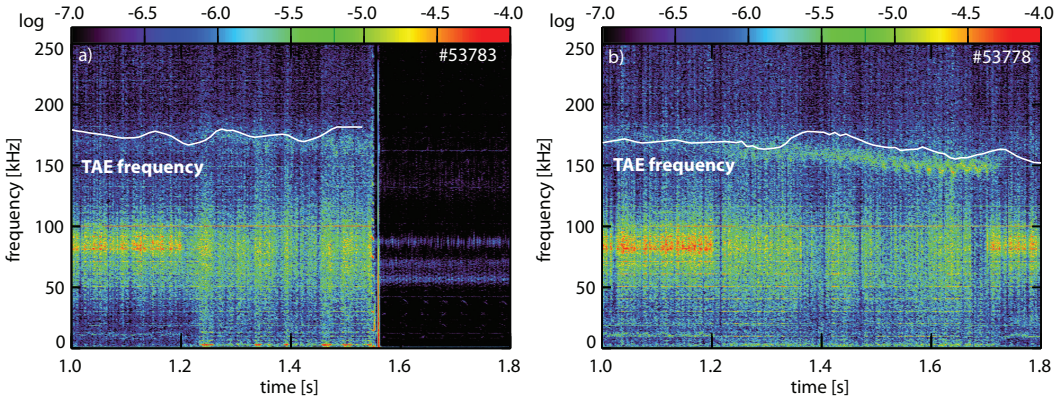

FIG. 18: Magnetic spectrograms for discharges #53783 (on-axis) and #53778 (off-axis). The estimated TAE frequency for a mode at the q=2.75 surface is plotted in white.

appear that are also present after the disruption in discharge #53783, indicating that this is a machine related perturbation. At even higher frequencies, a $n = 2$ mode is discerned that might be explained by toroidicity induced Alfvén eigenmodes (TAEs). TAEs are well known to be excited by fast ion with velocities in the range of one third of the Alfvén velocity which refers to a fast-ion energy of about 30 keV for these discharges. The theoretical frequencies of (m=5,n=2) TAE modes at the q=2.75 surface are plotted considering the formula from [28] for non-circular plasmas. These theoretical frequencies agree well with the experiment and suggest that NBI heating at TCV may drive TAE modes unstable. However, the modes are weaker but also present before the application of NBI and the observed band width of frequencies (30 kHz) is larger than typically expected from pure fast-ion driven TAE modes (∼2 kHz). Therefore, these modes could also be driven by fast electrons or turbulence, as observed previously by [29]. It is, thus, also possible that small-scale turbulence affects the fast-ion confinement at TCV, which is expected at high electron temperatures combined with low fast-ion energies [7]. This is the case at TCV and must be probed in MHD quiescent plasmas. Further studies of the fast-ion transport at TCV will therefore be the subject of future investigations.

5 Summary and discussion

Experiments with 1 MW of nominal NBI power (25 keV, deuterium) have been performed for L-mode plasma configurations with very low electron densities and high electron temperatures. The TRANSP code has been applied to simulate the fast-ion slowing down distribution and to compare predicted loop voltages and toroidal beta values with the measurements. The best agreement with the experiment is obtained by a model including strong fast-ion losses such that only 15% of the nominal beam power provides heating of the bulk (thermal) plasma. The fast-ion losses are required even to perform TRANSP

simulations as, otherwise, the fast-ion density becomes larger than the total deuterium ion density. The observed weak modification of the kinetic profiles also agrees with the Kaye confinemnt scaling for L-modes for low effective NBI heating efficiencies. In addition, synthetic spectra from FIDASIM using TRANSP predictions match active FIDA measurements using a poloidal spectroscopic view.

The reduction of the predicted fast-ion density is obtained by assuming anomalous fast-ion transport in the TRANSP simulations or by strong charge exchange losses with background neutrals. The presence of large neutral densities is directly supported by passive FIDA signal levels from toroidal lines of sight and from the absolute neutral fluxes measured by a compact neutral particle analyzer. This shows that charge exchange losses have a significant effect on the fast-ion density and NBI heating efficiency at TCV when the electron density is low. This finding is important, e.g. for future power balance analysis at TCV but also at other devices such as ASDEX Upgrade where charge-exchange losses have not yet been considered in the simulations [30].

The impact of charge exchange losses cannot, as yet, be characterized accurately enough to draw clear conclusions on the level of anomalous fast-ion transport. Further investigations of of the charge-exchange loss channel are required, including simulations using EMC3-Eirene [31] and detailed measurements of the neutral particle analyzer at TCV [13].This will allow one to quantify the fast-ion redistribution induced by high frequency MHD activity, as observed during NBI heating and tentatively attributed to toroidicity induced Alfvén eigenmodes or by turbulence that might affect the fast particles. This provide a challenging target for theoretical models and provide much needed insight for extrapolation to burning plasma regimes.

6 Acknowledgment

This work has been carried out within the framework of the EUROfusion Consortium and has received funding from the Euratom research and training programme 2014-2018 under grant agreement No 633053. The views and opinions expressed herein do not necessarily reflect those of the European Commission.

References

[1] HAWRYLUK, R. et al., Physics of Plasmas Close to Thermonuclear Conditions **1** (1980) 19.

[2] HEIDBRINK, W. W., Physics of Plasmas **15** (2008).

[3] GARCIA-MUNOZ, M. et al., Nuclear Fusion **49** (2009) 085014.

[4] COLLINS, C. S. et al., Phys. Rev. Lett. **116** (2016) 095001.

[5] GEIGER, B. et al., Nuclear Fusion **54** (2014) 022005.

[6] JACOBSEN, A. S. et al., Plasma Physics and Controlled Fusion **58** (2016) 042002.

[7] HAUFF, T. et al., Phys. Rev. Lett. **102** (2009) 075004.

[8] HEIDBRINK, W. W. et al., Phys. Rev. Lett. **103** (2009) 175001.

[9] GOODMAN, T. et al., Nuclear Fusion **48** (2008) 054011.

[10] KARPUSHOV, A. N. et al., Fusion Engineering and Design **9697** (2015) 493 , Proceedings of the 28th Symposium On Fusion Technology (SOFT-28).

[11] KARPUSHOV, A. N. et al., Fusion Engineering and Design **84** (2009) 993 , Proceeding of the 25th Symposium on Fusion Technology(SOFT-25).

[12] BEHN, R. et al., Review of Scientific Instruments **70** (1999).

[13] KARPUSHOV, A. N. et al., Review of Scientific Instruments **77** (2006).

[14] HEIDBRINK, W. W. et al., Plasma Physics and Controlled Fusion **46** (2004) 1855.

[15] DUVAL, B. P. et al., Physics of Plasmas **15** (2008).

[16] SALEWSKI, M. et al., Plasma Physics and Controlled Fusion **56** (2014) 105005.

[17] SALEWSKI, M. et al., Nuclear Fusion **54** (2014) 023005.

[18] SALEWSKI, M. et al., Nuclear Fusion **56** (2016) 106024.

[19] PANKIN, A. et al., Computer Physics Communications **159** (2004) 157 .

[20] WESTERHOF, E., Rijnhuizen Report (1989) 89.

[21] LIN-LIU, Y. R. et al., Physics of Plasmas (1994-present) **4** (1997) 4179.

[22] SAUTER, O. et al., Physics of Plasmas (1994-present) **6** (1999) 2834.

[23] CODA, S. et al., Nuclear Fusion **43** (2003) 1361.

[24] TAMOR, S., Journal of Computational Physics **40** (1981) 104 .

[25] HEIDBRINK, W. et al., Commun. Comput. Phys. **10** (2011) 716.

[26] STIX, T. H., Plasma Physics **14** (1972) 367.

[27] KAYE, S. et al., Nuclear Fusion **37** (1997) 1303.

[28] FESENYUK, O. P. et al., Physics of Plasmas **20** (2013).

[29] MARASCHEK, M. et al., Phys. Rev. Lett. **79** (1997) 4186.

[30] GEIGER, B. et al., Plasma Physics and Controlled Fusion **57** (2015) 014018.

[31] LUNT, T. et al., Plasma Physics and Controlled Fusion **56** (2014) 035009.